Improved optical transparency of calcium-doped ZnO thin films

İ. POLAT[a,*], S. YILMAZ [b], M. TOMAKIN[c], E. BACAKSIZ[d]
[a]*Department of Energy Systems Engineering, Faculty of Technology, Karadeniz Technical University, Trabzon, Turkey*
[b]*Department of Materials Engineering, Faculty of Engineering, Adana Alparslan Türkeş Science and Technology University, Adana, Turkey*
[c]*Department of Physics, Faculty of Arts and Sciences, Recep Tayyip Erdogan University, Rize, Turkey*
[d]*Department of Physics, Faculty of Sciences, Karadeniz Technical University, Trabzon, Turkey*

ZnO thin films with various Ca-doping contents were produced by spray pyrolysis. X-ray diffraction results showed that all samples had a hexagonal structure. Morphological analysis indicated that all films had granular topography. The best transparency was obtained for 2 at.% Ca-doped ZnO samples. Band gap of ZnO thin films was found to be 3.22 eV and didn't change with increasing of Ca-doping. Photoluminescence data indicated that all samples had four emission peaks. Electrical measurements revealed that Ca-doping resulted in a gradual improvement of carrier density and consequently a decrement of resistivity, which is important for application areas in opto-electronics.

(Received August 22, 2018; accepted June 14, 2019)

Keywords: Ca-doped ZnO, Thin films, Morphology, Transparency, Carrier concentration

1. Introduction

ZnO semiconductor (a band gap of 3.36 eV at room temperature) has recently attracted a great deal of attention because of its unique properties such as high optical transparency in the visible region, large exciton binding energy of 60 meV, nontoxic nature, excellent electrical conductivity and good chemical stability. These properties make it a promising material in the applications of optoelectronics, photonics and sensors [1-5]. ZnO materials can be produced a variety of methods including pulsed laser deposition (PLD) [6], chemical vapor deposition (CVD) [7], magnetron sputtering [8] and spray pyrolysis [9]. Of these methods, spray pyrolysis is particularly attractive one with simple and low-cost equipment, mass production and it can be used for large area production on glass and conductive substrates. On the other hand, this method ensures an advantage of doping atoms in the host matrix such as Mn, Na and Al etc. [10-12]. Doping is a good alternative way in controlling the physical properties of semiconductors like crystal structure, electrical, optical characteristics and surface morphology etc., which is suitable route to enhance their device applications. Until recently, there are lots of papers concerning about rare-earth, transition metal and nonmetal-doped ZnO to improve the optical and electrical properties of ZnO for different application areas. For instance, Hjiri and co-workers synthesized undoped, Ca- and Al-doped ZnO nanoparticles by sol-gel method and fabricated conductometric ZnO sensors. They investigated the effect of response to CO and CO_2 gases on the produced specimens and found that Ca-doped ZnO sensor demonstrated good response to CO_2 while Al-doped ZnO indicated high response towards CO [13]. Yu at al. successfully fabricated high-performance transparent Ca-doped ZnO thin film transistors. They studied the influence of substrate temperature on Ca-doped ZnO thin film transistor [14]. Qasim and co-workers grew ZnO and Ca-doped ZnO nanoparticles via solution precipitation method and used them as the electron transport layer in perovskite light-emitting diodes [15]. As can be seen from the literature review, though there have been published some works on Ca-doped ZnO system by different methods, spray pyrolysis fabricated Ca-doped ZnO thin films haven't been studied yet. Therefore, in this paper, undoped and Ca-doped ZnO thin films were produced by spray pyrolysis technique on glass slides and their structural, optical and electrical properties were systematically examined as a function of Ca-doping content. To characterize some physical properties of undoped and Ca-doped ZnO films, X-ray diffraction (XRD) and scanning electron microscopy (SEM) analyzes, UV-Vis and photoluminescence (PL) measurements and four-point method were used.

2. Experimental details

In this study, zinc nitrate hexahydrate $[Zn(NO_3)_2.6H_2O]$ and calcium acetate $[Ca(CH_3COO)_2.xH_2O]$ without further purification were chosen as precursors. Undoped and Ca-doped ZnO films ($Zn_{1-x}Ca_xO$; x=0.00, 0.01, 0.02, 0.03, 0.04, 0.05) were produced by spray pyrolysis method onto glass slides.

Prior to deposition of samples, glass slides were in turn ultrasonically rinsed with soap, acetone and distilled water about 10 minutes and then dried by compressed air. A solution of 0.1 M concentration was prepared with $Zn(NO_3)_2.6H_2O$ salt in distilled water to synthesize undoped ZnO thin films while doping process was achieved by adding of $Ca(CH_3COO)_2.xH_2O$ salt into above prepared solution to fabricate Ca-doped ZnO films with various doping contents. Prepared solutions were vigorously stirred at magnetic stirrer and then were sprayed onto preheated substrates. Deposition time and substrate temperature were adjusted to be 30 minutes and 400°C, respectively. More details of spray pyrolysis technique can be found in one of our earlier studies [16]. After deposition, it was shown that obtained films were good adhesion to glass slides for all specimens.

The influence of crystal structure, surface morphology and elemental analysis for fabricated films were investigated by X-ray diffraction (Rikagu D/MAX-IIIC difractometer) and scanning electron microscopy (Jeol JMS-6610), respectively. Transmittance measurements in the range of 300-1000 nm and Photoluminescence data with an excitation wavelength of 325 nm were recorded by means of a spectrophotometer (SpecraMax M5) at the room temperature. Resistivity and carrier concentration of thin films were measured by Hall Effect and Van der Pauw techniques.

3. Results and discussion

XRD results of undoped and Ca-doped ZnO thin films are showed in Fig. 1 (a)-(f). It is understood from Fig. 1(a) that undoped ZnO indicates four reflection peaks located at diffraction angles of 31.74°, 34.44°, 36.26° and 47.52° in the pattern, which correspond to (100), (002), (101), (102) planes, respectively. Also, the strongest peak in the pattern is along (002) reflection plane, indicating a preferential orientation along this plane. All the peaks are well matched to the hexagonal ZnO structure with a JCPDS card no. 36-1451. Fig. 1 (b)-(e) illustrate the XRD patterns of 1, 2, 3 and 4 at.% Ca-doped ZnO films, respectively. With increasing of Ca-doping level from 1 at.% to 4 at.%, intensity of (002) peak slightly increased. Such an increase in the intensity of (002) peak by Ca-doping may be commended as an improvement of crystal quality. Srivastava et al. found a similar behavior of with the rise of Ca-doping level for Ca-doped ZnO nanocrystalline films synthesized by screen printing route [17]. Once Ca-doping level is further increased to 5 at.%, intensity of (002) peak decreased as shown in Fig. 1(f), leading to the creation of crystal defects in the ZnO matrix that is handled in the below discussion like SEM [18]. However, peak positions of the samples aren't significantly altered. Additionally, it isn't observed any peaks involving metallic calcium or its complex in the ZnO within detection of XRD limit, meaning that Ca atoms are successfully resolved in the ZnO matrix. Table 1 shows lattice constants of ZnO and Ca-doped ZnO thin films. As shown in Table 1, lattice constants of *a* and *c* for undoped ZnO were calculated as 0.325 and 0.520 nm, respectively.

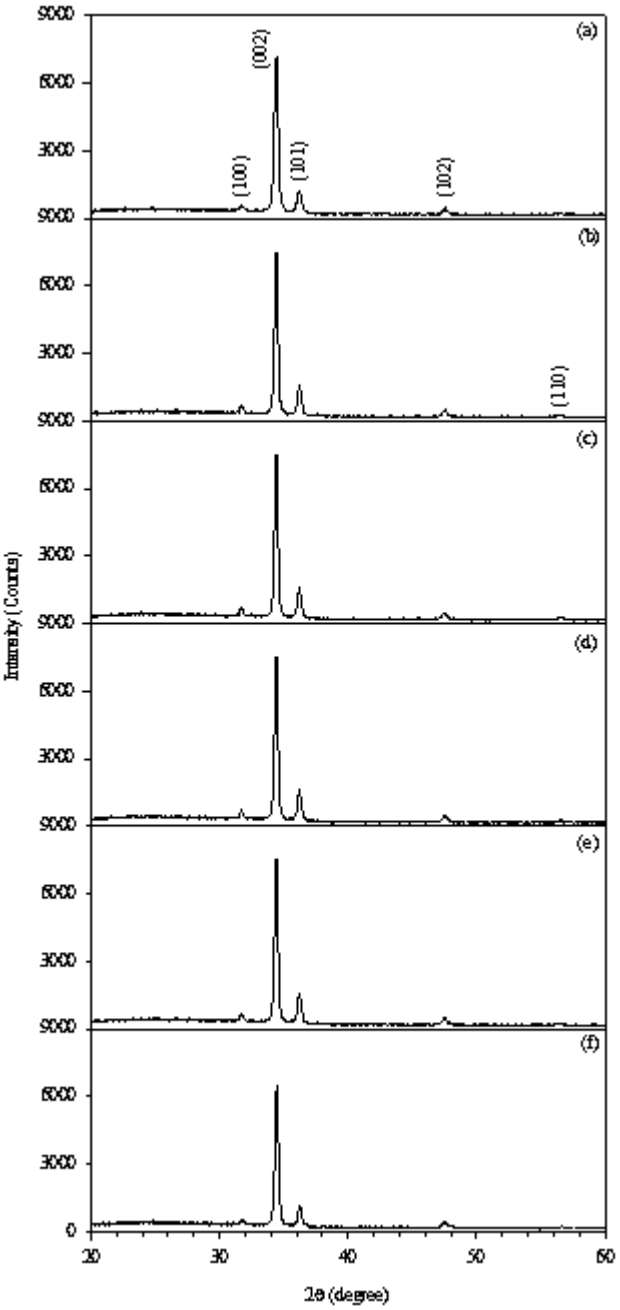

Fig. 1. XRD results of (a) ZnO and Ca-doped ZnO thin films for (b) 1 at.%, (c) 2 at.%, (d) 3 at.%, (e) 4 at.%, (f) 5 at.%

Lattice constant values of ZnO thin films aren't seriously changed after doping with Ca atoms. It might be expected to see an increment in the lattice constants of ZnO films by the increase of Ca-doping if Ca^{2+} ions substitute by Zn^{2+} sites in ZnO matrix because ionic radius of Ca^{2+} (0.99 Å) is larger than that of Zn^{2+} (0.74 Å). However, it is known that modification in the lattice constant depends on various parameters like the introduction of impurities with different ionic radius in the lattice, uniform stress, shift in stoichiometry, difference

between thermal expansion coefficient of ZnO and substrate, etc. [18]. For these reasons, it can be said that no change in the lattice parameters in the present study takes place due to the combined effect in above mentioned competing effects, concluding an either increasing or decreasing value of lattice parameters [19]. Crystal size of films is determined by using Scherrer formula [20] and obtained data are summarized in Table 1. It is seen from Table 1 that crystal size of undoped ZnO film is calculated to be 24.8 nm. As compared to undoped ZnO, Ca-doped ZnO samples exhibit slightly bigger *D* values.

Table 1. Lattice constants and crystallite sizes of ZnO and Ca-doped ZnO thin films

Sample	**Lattice parameters**		**Crystallite size** *D* (nm)
	a (nm)	*c* (nm)	
ZnO	0.325	0.520	24.8
1 at.% Ca-doped ZnO	0.325	0.521	29.0
2 at.% Ca-doped ZnO	0.325	0.520	28.6
3 at.% Ca-doped ZnO	0.325	0.520	26.6
4 at.% Ca-doped ZnO	0.326	0.521	28.3
5 at.% Ca-doped ZnO	0.325	0.521	26.3

SEM photographs of undoped and Ca-doped ZnO samples were given in Fig. 2 (a)-(f). It can be seen from Fig. 2(a) that undoped ZnO thin films have a compact morphology. The distribution of grains is homogeneous through the samples. With increment of Ca-doping levels from 1 at.% to 4 at.%, as indicated in Fig. 2(b)-(e), it is observed that a denser and more uniform morphology with smaller grains are formed, leading to an increment in the total length of grain boundaries. As ZnO films is doped by 5 at. % Ca content (Fig. 2(e)), the surface morphology of films substantially changes. It is noticeable that the film doesn't exhibit homogenous grain size distribution and some small grains aggregate to form bigger ones. Thus, the surface of films is covered by grains with the smallest in size and some voids also appear which is due to the formation of more deformation in the sample that is in accordance with XRD results, approving introduction of more Ca atoms in ZnO structure. As previously discussed in Fig. 1(f), once ZnO thin films are doped by 5 at.% Ca atoms, intensity of (002) peak decreases in comparison with other Ca-dopings, implying that the crystal quality deteriorates. Addition of Ca into ZnO generally leads to a reduction in the grain size that was also reported by Santoshkumar et al. for Ca-doped ZnO nanorods produced by hydrothermal route [21].

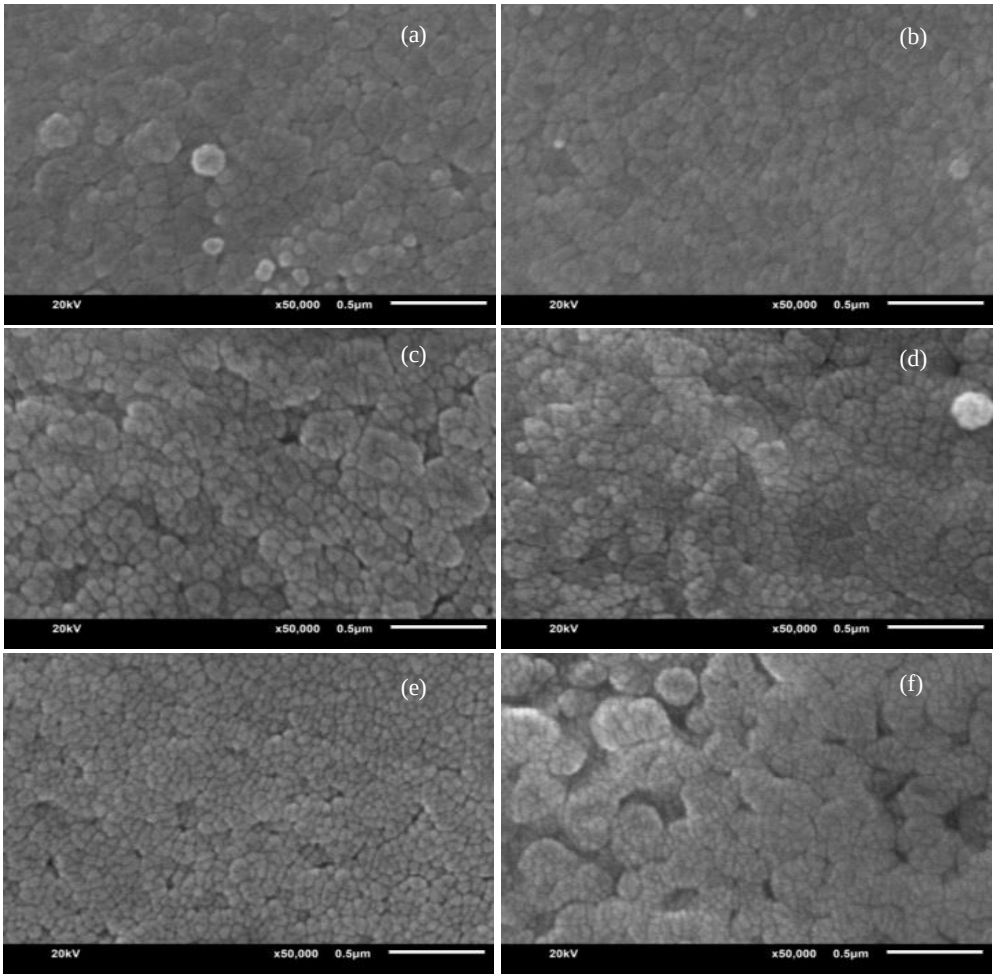

Fig. 2. SEM photographs of (a) ZnO and Ca-doped ZnO thin films for (b) 1 at.%, (c) 2 at.%, (d) 3 at.%, (e) 4 at.%, (f) 5 at.%

To investigate the composition of undoped and Ca-doped ZnO films, EDS measurement is conducted. Fig. 3 displays the EDS survey spectrum of 3 at.% Ca-doped ZnO film. From Fig. 3, it is seen that specimen is composed of Ca, Zn and O, which confirms the Ca-doping in the host matrix of ZnO films. The real compositions of Zn, O and Ca atoms for undoped and Ca-doped ZnO thin films are given in Table 2. It is found that as the nominal Ca-doping content in ZnO films increases, the real Ca-content rises as well and the actual Ca-contents in the matrix of ZnO is lower than those of nominal ones, suggesting that the resolution of Ca atoms in ZnO matrix is low. It is also seen that the ratio of Zn/O for undoped ZnO film is lower than one, implying that the film is nonstoichiometric. Thus, this causes lack of zinc and excess of oxygen, resulting in the creation of zinc vacancy and oxygen interstitial defects [22]. As Ca-content in ZnO is increased, the ratio of Zn/O approaches to one when compared to the undoped ZnO, implying that more stoichiometric films are obtained.

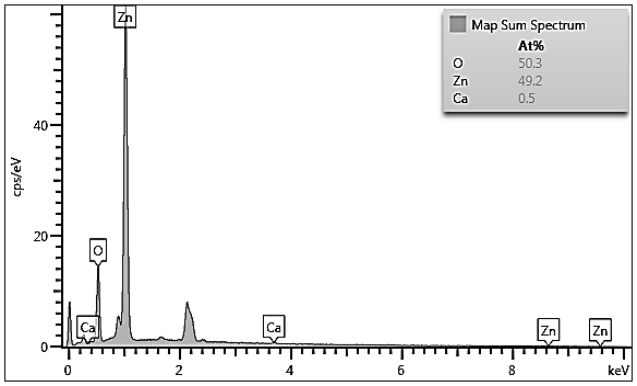

Fig. 3. EDS survey spectrum of 3 at.% Ca-doped ZnO thin films

Table 2. Real and nominal atomic concentration of Zn, O and Ca atoms in ZnO and Ca-doped ZnO thin films

Sample	Zn	O	Ca
ZnO	48.2	51.8	-
1 at.% Ca-doped ZnO	49.2	50.5	0.3
2 at.% Ca-doped ZnO	49.3	50.3	0.4
3 at.% Ca-doped ZnO	48.2	50.3	0.5
4 at.% Ca-doped ZnO	48.5	50.9	0.6
5 at.% Ca-doped ZnO	48.1	51.2	0.7

Transmittances of undoped and Ca-doped ZnO films are measured as a function of wavelength and results in the range of 300-1000 nm are given in Fig. 4. As can be seen in Fig. 4, transmittance is seriously affected by Ca-doping in the visible range of the spectrum. Undoped ZnO films have a transmittance curve displaying an ascending behavior with a maximum value of 77 % at 1000 nm. With 1 at.% Ca-doping, transmittance value slightly decreases to 75 % at the same wavelength value. The reason for such a decrement might be ascribed to decreasing grain in size which induces more grain boundaries, resulting in the more scattering. Bacaksız and co-workers observed an analogous outcome for ZnO microrods prepared by spray pyrolysis technique with ascending of Al-doping level [23]. As ZnO is doped with 2 at.% Ca, transmittance enhances and reaches a maximum value of 83 % at 1000 nm. The enhancement in *T* value could be related to the enhancement of crystal quality (disputed in XRD), implying a better optical quality of thin film. High transparency in the visible range is very important parameter for applications in opto-electronic devices [24]. After doping level of Ca towards 3 and 4 at.%, transmittance value exhibits a drop throughout all the spectrum though their values are higher than that of undoped one. Further increasing Ca-doping levels up to 5 at.% gives rise to a transmittance value of 79 % at 1000 nm. This behavior can be explained by the further increasing Ca-doping level. That is, when more Ca atoms are introduced in the ZnO structure more distortion is created, causing more crystal defects [25].

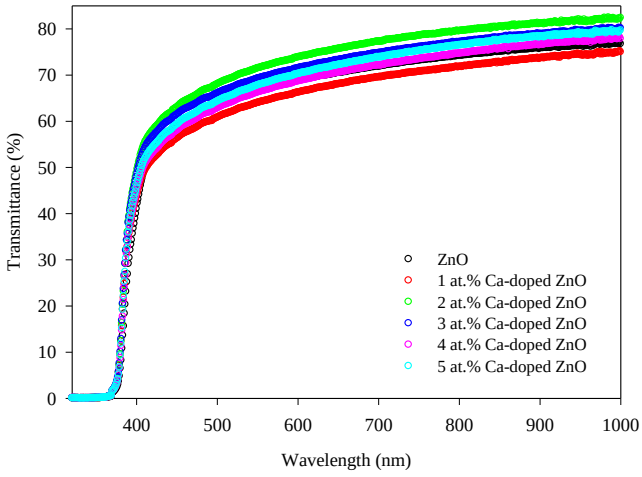

Fig. 4. Transmittance data of ZnO and Ca-doped ZnO thin films

Optical band gap (E_g) of undoped and Ca-doped ZnO thin films is determined using Tauch's relationship [26] and resultant data are given in Fig. 5. As can be seen from this figure, band gap value of undoped ZnO film is found to be 3.22 eV. This value is smaller than that of ZnO bulk materials (3.37 eV). The difference band gap between thin film and bulk is probably due to some crystal defects such as existence of grain boundaries and imperfections in polycrystalline thin films [27,28]. After doping with Ca atoms, the band gap values of all Ca-doped ZnO samples don't significantly change. Mahdhi and co-workers fabricated films by rf magnetron sputtering method and they reported that the band gaps of Ca-doped ZnO films increased from 3.30 to 3.42 eV with increasing Ca doping concentration [29]. On the other hand, Slama at al. synthesized Ca-doped ZnO by sol-gel technique and they found that the band gap of pure ZnO was 3.22 eV and it

increased up to 3.30 eV for 1 at.% Ca doping and further increase in doping content of 5 at.% Ca caused a decrement as 3.02 eV [30]. It can be summarized from the reported papers that there has been no consensus in the band gap results of ZnO upon Ca-doping.

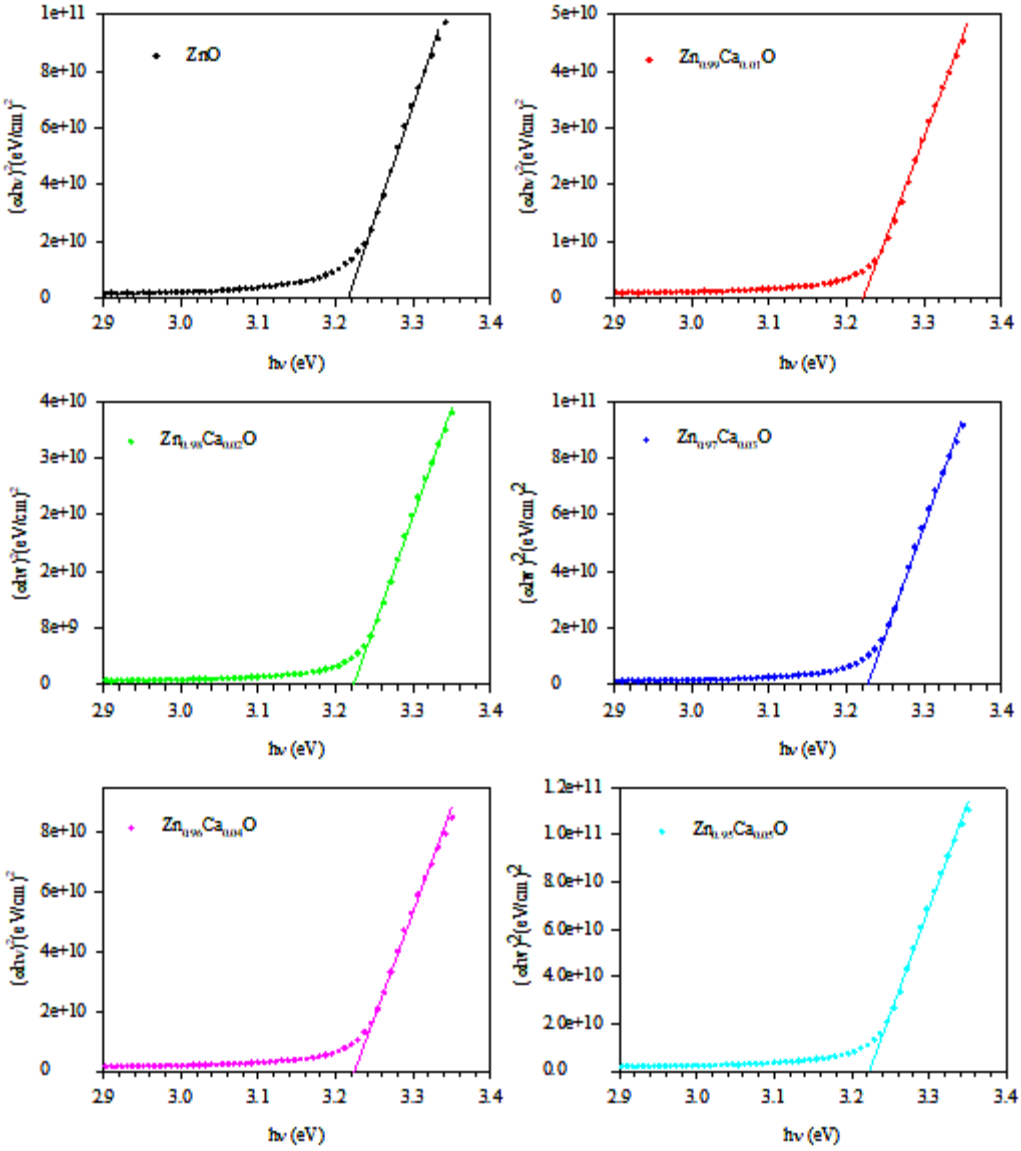

Fig. 5. Tauc's graphs of ZnO and Ca-doped ZnO thin films

The room-temperature photoluminescence (RTPL) spectra of undoped and Ca-doped ZnO thin films are recorded at excitation wavelength of 325 nm and illustrated in Fig. 6. As can be seen Fig. 6, the spectrum of undoped ZnO thin film is composed of four main peaks. The first one is near band emission peak located at 392 nm (3.16 eV) which is attributed to the recombination of free excitons [31]. The second broad one is visible blue light (VBL) emission peak between 400 nm and 500 nm, which is generally ascribed to intrinsic defects like as zinc interstitial (Zn_i), zinc vacancy (V_{Zn}) and singly negatively charged Zn vacancy (V_{Zn}^-). VBL band is composed of three satellite peaks corresponding to violet emission at 416 (2.95 eV), a blue emission 441 nm (2.81 eV) and blue-green emission at 480 nm (2.58 eV) peak, which are ascribed to Zn_i, V_{Zn}, and V_{Zn}^-, respectively [32, 33]. The third broad one (green emission at 531 nm, 2.33 eV) is located the range of 500 nm and 550 nm, which is referred to oxygen vacancy (V_o) [34]. The fourth another broad peak is observed in the range from 550 nm to 700 nm and can be attributed to presence of interstitial oxygen vacancies (O_i) [35]. It is also seen from Fig. 6, the doping of Ca in the ZnO structure doesn't change the general appearance of the PL spectrum of ZnO thin films. Furthermore, it isn't appeared any extra emission peak in the PL spectrum, which implies that no additional defects are formed when ZnO thin films are doped with Ca atoms. However, peak intensities of the Ca-doped ZnO throughout the spectra decrease compared to spectrum of ZnO thin films. The reason for this decrement may be considered by the fewer defect density for Ca-doped ZnO samples (as conformed by EDS results), which is formed

by the radiative recombinations between V_{Zn} and O_i defects, giving rise to a decline in the number of both kind of defects [36].

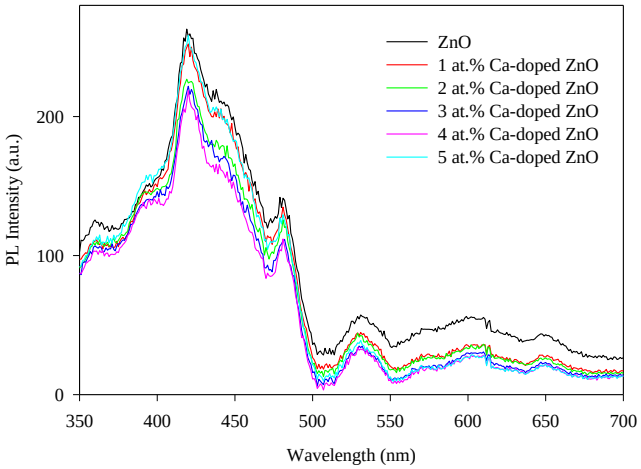

Fig. 6. RTPL plots of ZnO and Ca-doped ZnO thin films

The electrical properties of undoped and Ca-doped ZnO thin films are given in Table 3. As can be seen in Table 3, the minimum value of carrier density (n) and maximum value of resistivity (ρ) were found as 2.44×10^{13} cm^{-3} and 8.08×10^{4} Ω.cm, respectively. Ca-doping in ZnO thin films results in a gradual improvement of carrier density and consequently a decrement of resistivity. Compared to undoped ZnO, 2, 3 and 4 at.% Ca-doped ZnO thin films exhibits higher carrier concentration and lower resistivity, which may be attributed to an improvement of crystallinity because the increasing of Ca-doping content brings about the fewer defect density (argued in XRD). An analogous conclusion was reported by Mandhi and co-workers for Ca-doped ZnO thin films grown by rf magnetron sputtering with the boost of Ca-doping level [37]. On the other hand, a minimum resistivity of 1.14×10^{4} Ω.cm is obtained for 5 at.% Ca-doped ZnO thin films, which corresponds to a maximum concentration of 1.70×10^{14} cm^{-3}, respectively. These enhancements could be related to the drop in the population of intrinsic defects observed in PL results for Ca-doped ZnO thin films.

Table 3. Carrier densities and resistivities of ZnO and Ca-doped ZnO thin films

Sample	Carrier density (cm^{-3})	Resistivity (Ω.cm)
ZnO	2.44×10^{13}	8.08×10^{4}
1 at.% Ca-doped ZnO	5.15×10^{13}	4.46×10^{4}
2 at.% Ca-doped ZnO	5.98×10^{13}	2.93×10^{4}
3 at.% Ca-doped ZnO	7.36×10^{13}	2.24×10^{4}
4 at.% Ca-doped ZnO	1.11×10^{14}	1.33×10^{4}
5 at.% Ca-doped ZnO	1.70×10^{14}	1.14×10^{4}

4. Conclusions

Undoped and Ca-doped ZnO thin films were fabricated by simple spray pyrolysis method onto glass substrates. It was seen from XRD and SEM analysis that undoped and Ca-doped thin films had a wurtzite structure and Ca-doping improved the crystal quality up to 4 at.% and more doping of Ca deteriorated crystal structure. It was found from morphological investigation that up to 4 at.% Ca doping, denser and more uniform morphology were formed. As ZnO films was doped by 5 at. % Ca content, ZnO thin films exhibited the smallest grain size and some voids started to appear. Optical transmittance values of all films were over 70% in the visible wavelength region. With respect to undoped ZnO, the band gap values of all Ca-doped ZnO samples didn't significantly change. It was observed from RTPL measurements that all samples had near band emission peak, visible blue light (VBL) emission peak, green emission peak and a broad peak ranging from 550 nm to 700 nm. From electrical measurements, a minimum resistivity and a maximum concentration were obtained to be 1.14×10^{4} Ω.cm and 1.70×10^{14} cm^{-3}, respectively for 5 at.% Ca-doped ZnO thin films.

References

[1] L. W. Wang, Y. F. Kang, X. H. Liu, S. M. Zhang, W. P. Huang, S. R. Wang, Sens. Actuators B **162,** 237 (2012).
[2] İ. Polat, S. Yılmaz, E. Bacaksız, Y. Atasoy, M. Tomakin, J. Mater. Sci. - Mater Electron. **25,** 3173 (2014).
[3] M. Raula, M. H. Rashid, T. K. Paira, E. Dinda, T. K. Mandal, Langmuir **26**, 8769 (2010).
[4] H. Bai, X. Li, C. Hu, X. Zhang, J. Li, Y. Yan, G. Xi, Sci. Rep. **3**, 2204 (2013).
[5] Z. L. Wang, J. Phys.: Condens. Matter. **16**, R829 (2004).
[6] Y. Sun, G. M. Fuge, M. N. R. Ashfold, Chem. Phys. Lett. **396**, 21 (2004).
[7] S.-W. Kim, S. Fujita, H.-K. Park, B. Yang, H.-K. Kim, D. H. Yoon, J. Cryst. Growth **292**, 306 (2006).
[8] P. Y. Dave, K. H. Patel, K. V. Chauhan, A. K. Chawla, S. K. Rawala, Procedia Technol. **23**, 328 (2016).
[9] E. Bacaksiz, S. Aksu, G. Çankaya, S. Yılmaz, İ. Polat, T. Küçükömeroğlu, A. Varilci, Thin Solid Films **519,** 3679 (2011).
[10] R. Chandramohana, T. A. Vijayan, S. Arumugam, H. B. Ramalingam, V. Dhanasekaran, K. Sundaram, T. Mahalingam, Mater. Sci. Eng. B **176**, 152 (2011).
[11] İ. Polat, J. Mater. Sci. – Mater. Electron. **25,** 3721 (2014).
[12] J. Lang, Q. Han, C. Li, J. Yang, X. Li, L. Yang, D. Wang, H. Zhai, M. Gao, Y. Zhang, X. Liu, M. Wei, Appl. Surf. Sci. **256**, 3365 (2010).
[13] M. Hjiri, N. Zahmouli, R. Dhahri, S. G. Leonardi, L. El Mir, G. Neri, J. Mater. Sci.: Mater. Electron.

28, 9667 (2017).
[14] W. Yu, D. Han, P. Shi, Y. Cong, Y. Zhang, J. Dong, X. Zhou, L. Huang, G. Cui, S. Zhang, X. Zhang, Y. Wang, Electron. Lett. **51**, 1286 (2015).
[15] K. Qasim, B. Wang, Y. Zhang, P. Li, Y. Wang, S. Li, S.-T. Lee, L.-S. Liao, W. Lei, Q. Bao, Adv. Funct. Mater. **27**, 1606874 (2017).
[16] E. Bacaksiz, G. Çankaya, İ. Polat, S. Yılmaz, C. Duran, M. Altunbaş, J. Alloys Compd. **496,** 560 (2010).
[17] A. Srivastava, R. K. Shukla, K. P. Misra, Cryst. Res. Technol. **46**, 949 (2011).
[18] T. Das, B. K. Das, K. Parashar, S. K. S. Parashar, Acta Phys. Pol. A **130**, 1358 (2016).
[19] I. Polat, S. Aksu, M. Altunbas, S. Yılmaz, E. Bacaksız, J. Solid State Chem. **184**, 2683 (2011).
[20] P. Scherrer, Nachr. Ges. Wiss. Göttingen **26**, 98 (1918).
[21] B. Santoshkumar, S. Kalyanaraman, R. Vettumperumal, R. Thangavel, I. V. Kityk, S. Velumani, J. Alloys Compd. **658**, 435 (2016).
[22] J. I. Contreras-Rascon, M. E. Linares-Aviles, J. Diaz-Reyes, J. F. Sanchez-Ramirez, J. E. Flores-Menad, R. S. Castillo-Ojeda, M. C. Peralta-Clara, J. S. Veloz-Rendon, Rev. Mex. Fis. **64**, 240 (2018).
[23] E. Bacaksiz, S. Aksu, S. Yılmaz, M. Parlak, M. Altunbaş, Thin Solid Films **518**, 4076 (2010).
[24] H. Mahdhi, K. Djessas, Z. Ben Ayadi, Mater. Lett. **214**, 10 (2018).
[25] P. Velusamy, R. Ramesh Babu, K. Ramamurthi, J. Viegas, E. Elangovan, J. Mater. Sci.- Mater. Electron. **26**, 4152 (2015).
[26] J. Tauc, R. Grigorovici, A. Vancu, Phys. Status Solidi B **15**, 627 (1966).
[27] S. Zandi, P. Kameli, H. Salamati, H. Ahmadvand, M. Hakimi, Phys. B: Condensed Mater. **406**, 3215 (2011).
[28] D. Bao, H. Gu, A. Kuang, Thin Solid Films **312**, 37 (1998).
[29] H. Mahdhi, J. L. Gauffier, K. Djessas, Z. Ben Ayadi, Optik **137**, 156 (2017).
[30] R. Slama, J. El Ghoul, K. Omri, A. Houas, L. El Mir, F. Launay, J. Mater. Sci. – Mater. Electron. **27**, 7939 (2016).
[31] K. Vanheusden, W. L. Warren, C. H. Seager, D. R. Tallant, J. A. Voigt, B. E. Gnade, J. Appl. Phys. **79**, 7983 (1996).
[32] H. Liu, X. Zhang, L. Li, Y. X. Wang, K. H. Gao, Z. Q. Li, R. K. Zheng, S. P. Ringer, B. Zhang, X. X. Zhang, Appl. Phys. Lett. **91**, 072511 (2007).
[33] X. Zhang, W. H. Wang, L. Y. Li, Y. H. Cheng, X. G. Luo, H. Liu, Z. Q. Li, R. K. Zheng, S. P. Ringer, EPL **84**, 27005 (2008).
[34] N. Varghese, L. S. Panchakarla, M. Hanapi, A. Govindaraj, C. N. R. Rao, Mater. Res. Bull. **42**, 2117 (2007).
[35] M. Liu, A. H. Kitai, P. Mascher, J. Lumin. **54**, 35 (1992).
[36] S. Yılmaz, E. McGlynn, E. Bacaksız, Ş. Özcan, D. Byrne, M. O. Henry, R. K. Chellappan, J. Appl. Phys. **111,** 013903 (2012).
[37] H. Mahdhi, K. Djessas, Z. Ben Ayadi, Mater. Lett. **214**, 10 (2018).

*Corresponding author: ismlpolat@yahoo.com